Published online September 5, 2019

Gross Primary Production Estimation in Crops Using Solely Remotely Sensed Data

Yi Peng, Oz Kira,* Anthony Nguy-Robertson, Andrew Suyker, Timothy Arkebauer, Ying Sun, and Anatoly A. Gitelson*

ABSTRACT

Gross primary production (GPP) is a measure for crop productivity, indicating yield and expressing C exchange of agro-ecosystems. A multitude of satellite sensors at varying spatial and spectral resolution brings a possibility to use remotely sensed data for regional and global GPP estimation. More work is still needed to develop algorithms for GPP estimation applicable to multiple, if not all, vegetation types, phenological phases, and environmental conditions. This study employed neural networks (NN), multiple linear regressions (MLR), and vegetation indices (VI) to develop algorithms for GPP estimation based solely on remotely sensed data in two crops, maize (*Zea mays* L.) and soybean [*Glycine max* (L.) Merr.], with contrasting canopy architectures, leaf structures, and photosynthetic pathways. The focus of the study was to devise algorithms not requiring re-parameterization for different crop species. Data used in the models included in situ hyperspectral reflectance and satellite surface reflectance products. For the tested NN, MLR, and VI algorithms, the bands selected to obtain minimal errors in maize and soybean combined were mainly located in red edge and near infrared (NIR) spectral regions. For both in situ reflectance and satellite surface reflectance, a NN estimated GPP with normalized root mean square errors (NRMSE) below 14 and 18.7%, respectively, and VI using bands in red edge and NIR with NRMSE 15.6 and 20.4%, respectively. The results showed that the models based on the red edge and NIR bands may facilitate accurate assessments of crop GPP at multiple scales, from close range to satellite platforms.

Core Ideas

- The models using remotely sensed data allow accurate estimation of gross primary production in two crops.
- The optimal bands for gross primary production estimation in two crops were in near infrared and red edge regions.
- Vegetation indices with red edge and near infrared reflectance were generic for maize and soybean.

Published in Agron. J. 111:1–10 (2019)
doi:10.2134/agronj2019.05.0332

Copyright © 2019 The author(s). Re-use requires permission from the publisher.

Gross primary production is the amount of biomass C that plants produce in a given period of time. As such, it is the sum of the net primary production (NPP), that is, the net amount of useful biomass C produced by plants, and plant respiration (Re). We have quantified the relationship of cumulative growing season GPP (g C m^{-2} $season^{-1}$) and grain yield (g C m^{-2} $season^{-1}$) at the Nebraska AmeriFlux sites (US-Ne1, US-Ne2, and US-Ne3). The coefficient of determination (R^2) for this relationship over the first 14 yr of the project is 0.95. This includes both maize and soybean grown under irrigated and rainfed conditions and encompasses a wide variation in environmental conditions. Grain yield is arguably the single most important consideration for agricultural producers and, due to its close correlation with GPP, measurements of GPP are of great interest for evaluating crop yield (e.g., Reeves et al., 2005). Traditionally, field studies use tower eddy covariance systems (e.g., Baldocchi, 2003) to obtain GPP in croplands. However, such approaches bring results over a limited spatial coverage. Remote sensing, which provides observations at various scales, has been increasingly employed as a powerful and efficient tool for a diverse range of applications and studies related to agriculture management, precision farming, ecosystem monitoring, and climate change (Dorigo et al., 2007; D'Urso et al., 2010; Thenkabail et al., 2011; Hank et al., 2019).

Reflectance spectra of vegetation in the visible and NIR spectral range are governed by canopy biochemical and structural properties resulting in variable absorption and scattering. Thus, there is a link between spectral features of remotely sensed reflectance and vegetation biophysical parameters such as foliar pigment contents, fraction of absorbed photosynthetically active radiation (fAPAR), leaf area index (LAI), and GPP (Woolley,

Y. Peng, School of Remote Sensing and Information Engineering, Wuhan Univ., China, 430079; Y. Peng, Lab for Remote Sensing of Crop Phenotyping, Wuhan Univ., China, 430079; O. Kira and Y. Sun, Soil and Crop Sciences, School of Integrative Plant Science, College of Agriculture and Life Sciences, Cornell Univ., Ithaca, NY 14853; A. Nguy-Robertson, A. Suyker, and A.A. Gitelson, School of Natural Resources, Univ. of Nebraska-Lincoln, Lincoln, NE 68583; T. Arkebauer, Dep. of Agronomy and Horticulture, Univ. of Nebraska-Lincoln, Lincoln, NE 68583; A.A. Gitelson, Israel Institute of Technology (Technion), Haifa, Israel, 3200003. Received 1 May 2019. Accepted 10 July 2019. *Corresponding author (agitelson2@unl.edu, ok78@cornell.edu).

Abbreviations: Chl, chlorophyll; [Chl], chlorophyll content; GPP, gross primary production; LAI, leaf area index; MERIS, medium resolution imaging spectrometer; MLR, multiple linear regression; NEE, net ecosystem exchange; NIR, near infrared; NN, neural network; NRMSE, normalized root mean square error; OLCI, ocean and land color instrument; PAR, photosynthetically active radiation; RI, reliability index; TM/ETM+, thematic mapper or enhanced thematic mapper plus; UVE-PLS, uninformative variable elimination by partial least square regression; VI, vegetation index.

1971; Allen et al., 1973; Gitelson, 2011, 2018). The total canopy chlorophyll (Chl) content relates to both crop phenology and photosynthetic capacity (Whittaker and Marks, 1975; Ustin et al., 1999; Zarco-Tajeda et al., 2002). Thus, canopy Chl content [Chl] is one of the main factors indicating productivity of vegetation where GPP is governed by the photosynthetic pigment pool shared by crops, grasses, deciduous forests, and so on (e.g., Medina and Lieth, 1964; Gitelson et al., 2006a; Sakowska et al., 2014; Rossini et al., 2014).

A close and almost non-species-specific relationship (for maize and soybean) was found between GPP and canopy [Chl], defined as a product of leaf [Chl] and leaf area index (Gitelson et al., 2006b; Peng et al., 2011). A simple but robust model was then suggested for estimating crop GPP:

$$\text{GPP} = \text{canopy [Chl]} \times \text{PAR}_{\text{in}} \quad [1]$$

where PAR_{in} is the photosynthetically active radiation (PAR) incident on a horizontal surface above the canopy. Canopy [Chl] can be accurately retrieved from remotely measured canopy reflectance (Gitelson et al., 2003, 2005 ; Dash and Curran, 2004; Ciganda et al., 2009).

Several studies have explored estimation of GPP via the remote measurement of canopy [Chl]. Harris and Dash (2010) used the MERIS terrestrial chlorophyll index (MTCI), derived from MEdium Resolution Imaging Spectrometer (MERIS) satellite data, to estimate C flux in sites encompassing a wide variation in vegetation composition. Sakowska et al. (2014) used multispectral reflectance data to test different models for quantifying GPP in grassland and found that Chl-related indices, specifically the red edge Chl index, were the best GPP predictors. Sakamoto et al. (2011) quantified daily GPP in maize using daily shortwave radiation, derived from reanalysis data (North American Land Data Assimilation System, NLDAS-2) and Wide Dynamic Range Vegetation Index (WDRVI; Gitelson, 2004), derived from Moderate Resolution Imaging Spectroradiometer (MODIS) 250-m observations. However, shortwave radiation did not relate very closely to ground-observed PAR_{in} thus bringing significant uncertainties of GPP estimation (Sakamoto et al., 2011).

An improved GPP model based on Eq. [1] was introduced using potential photosynthetically active radiation ($\text{PAR}_{\text{potential}}$) instead of PAR_{in} for GPP estimation under clear sky conditions, specifically for satellite data (Gitelson et al., 2012):

$$\text{GPP} = \text{Canopy [Chl]} \times \text{PAR}_{\text{potential}} \quad [2]$$

The $\text{PAR}_{\text{potential}}$ is incident PAR under a condition of minimal atmospheric aerosol loading that can be easily obtained for each day of year for any location (Peng et al., 2013). The PAR_{in} fluctuates with daily weather conditions but daily GPP does not follow such high frequency variations, especially for clear sky conditions. It was found that the use of PAR_{in} in the model introduced noise and unpredictable uncertainties in GPP estimation (Gitelson et al., 2012; Sakamoto et al., 2011). Using $\text{PAR}_{\text{potential}}$ reduces this uncertainty to some degree. This model, Eq. [2], based on solely remotely sensed data, was tested using green Chl index as a proxy for total canopy [Chl] retrieved from surface reflectance products of Thematic Mapper or Enhanced Thematic Mapper Plus (TM/ETM+) Landsat images (Gitelson et al., 2012). The model was calibrated over three AmeriFlux cropland sites in Nebraska and was capable of predicting GPP in AmeriFlux sites in Minnesota, Iowa, and Illinois more accurately than the model based on PAR_{in}. Rossini et al. (2014), estimating GPP in high altitude grassland ecosystems, showed that the best results were obtained using the model driven by the product of red edge Chl index and $\text{PAR}_{\text{potential}}$. Peng et al. (2013) showed that GPP in maize and soybean could be accurately estimated using MODIS 250 m resolution data and $\text{PAR}_{\text{potential}}$ for clear sky weather conditions. In addition, they compared the models using PAR_{in} and $\text{PAR}_{\text{potential}}$ for GPP estimation with daily MODIS data over 8 yr under varying weather conditions. It was found that as more data taken under cloudy or hazy weather conditions were included, the accuracy of both models decreased but the use of $\text{PAR}_{\text{potential}}$ consistently brought higher accuracy until the difference between $\text{PAR}_{\text{potential}}$ and PAR_{in} was > 60%.

Canopy reflectance spectra are greatly affected by leaf structure, canopy architecture, and photosynthetic pathway. Thus, parameters of algorithms estimating crop GPP may vary considerably between different crops. When sensor field of view contains multiple crops, the use of the same algorithm for different crops may cause significant estimation uncertainties (Nguy-Robertson et al., 2014; Peng and Gitelson, 2012). It is unrealistic to have preknowledge of all crop types and then re-parameterize the algorithms for each crop especially at regional scales. Moreover, the discrepancy between the image spatial resolution and smaller sizes of fields may make it impossible to separate the detected signals originating from different species. Thus, algorithms applicable for different crops with no re-parameterization under different environments, not achieved yet, are crucial for improving estimation accuracy of GPP and might be beneficial also for ecological studies that explore more species in diverse environments.

Our primary objectives of this study are threefold: (i) to examine crop-specific differences affecting the algorithms based on the model Eq. [2] using in situ reflectance taken over rainfed and irrigated maize and soybean; (ii) to identify informative spectral bands for estimating GPP with emphasis on algorithms not-requiring re-parameterization for maize and soybean; and (iii) to assess the accuracy of GPP estimation using reflectance in simulated bands of satellites, and by surface reflectance products of satellite sensors TM/ETM+ Landsat and MERIS Envisat, as prototype of Ocean and Land Color Instrument (OLCI, Sentinel-3).

To accomplish the objectives, we applied NN, MLR, and VI for algorithm development based on the model Eq. [2] using data taken more than 8 yr of observation: (a) hyperspectral in situ reflectance, (b) reflectance simulated in spectral bands of TM/ETM+, MERIS MultiSpectral Imager (MSI, Sentinel-2), and OLCI, and (c) surface reflectance products of TM/ETM+ and MERIS. We evaluated the validity of the algorithms to estimate GPP in maize and soybean for each crop and crops combined with no re-parameterization for each crop.

MATERIALS AND METHODS

Study Area

Three AmeriFlux sites (US-Ne1, US-Ne2, and US-Ne3), located at the University of Nebraska-Lincoln Eastern Nebraska Research and Extension Center near Mead (Verma et al., 2005), were utilized in this study during growing seasons (from May–September)

2001 through 2008. They are approximately 60-ha fields within 4 km of each other. The US-Ne1 was planted with continuous maize and was equipped with a center pivot irrigation system. The US-Ne2 and US-Ne3 were planted with maize–soybean rotation, with one irrigated by a center pivot irrigation system (US-Ne2) and the other depending on rainfall (US-Ne3).

Ground Observation of Incident Photosynthetically Active Radiation and Calculated Potential Photosynthetically Active Radiation

In each study site, point quantum sensors (LI-190, LI-COR Inc., Lincoln, NE) were placed 6 m above the surface pointing toward the sky to measure PAR_{in} integrated to every hour. Daytime PAR_{in} values were computed by integrating the hourly measurements during a day when hourly PAR_{in} exceeded 1 μmol m^{-2} s^{-1}, and then presented in MJ m^{-2} d^{-1} (Turner et al., 2003).

The temporal behavior of PAR_{in} during the growing season includes low- and high-frequency variations. The former is due to seasonally decreased PAR_{in} since daylength in the northern hemisphere gradually decreases after the summer solstice (e.g., such decrease begins around 21 June for Nebraska). Since $PAR_{potential}$ depends solely on astronomical data (Weiss and Norman, 1985; Nguy-Robertson et al., 2015), we generated $PAR_{potential}$ profiles as a function of the day of year (DOY) for the Nebraska site locations. Based on the measured daytime PAR_{in}, for each DOY, $PAR_{potential}$ was assumed to be the maximal PAR_{in} value during eight consecutive days. The best-fit function of 8-d-maximal PAR_{in} vs. day of year (DOY) was then developed for $PAR_{potential}$ calculation of a given DOY (Gitelson et al., 2012; Peng et al., 2013).

In this study, we used a PAR_{in} constraint criterion to select days when sites were under "cloud-free" conditions with clear satellite images available. For the same sites in Nebraska that were used in this study, as well for sites in Minnesota, Iowa, and Illinois, it was found that about 90% of "cloud free" TM/ETM+ Landsat images were obtained when PAR_{in} was greater than 80% of $PAR_{potential}$ (Gitelson et al., 2012). Therefore, we focused our attention on days when PAR_{in} was above 80% of $PAR_{potential}$ and cloudiness coefficient was below 0.2 (Gitelson et al., 2015).

Gross Primary Production Inferred from Eddy Covariance Measurements

Each site is equipped with an eddy covariance tower and meteorological sensors with which the continuous measurements of CO_2 fluxes, water vapor, and energy fluxes were measured and integrated hourly. Fluxes measured during periods of insufficient turbulence/sensor malfunction were removed and gap-filled using standard techniques (Suyker et al., 2005). Daytime net ecosystem exchange (NEE) values were computed based on integrating the hourly CO_2 fluxes collected during a day when PAR_{in} exceeded 1μmol m^{-2} s^{-1}. Daytime estimates of ecosystem respiration (Re) were obtained from the night CO_2 exchange-temperature relationship (e.g., Xu and Baldocchi, 2003). The GPP was then obtained by subtracting Re from NEE as GPP = NEE – Re. This approach has been widely used in the context of tower flux measurements and is considered to provide reasonable estimates at the landscape level (details in Verma et al., 2005; Suyker et al., 2005).

In Situ Canopy Reflectance

Canopy reflectance was measured during the growing seasons of 2001 through 2008 using hyperspectral radiometers mounted on an all-terrain sensor platform (Rundquist et al., 2004, 2014). A dual-fiber optic system, with two inter-calibrated Ocean Optics USB2000 radiometers, was used to collect radiometric data in the range of 400 to 1000 nm at a spectral resolution of about 2 nm. One radiometer was equipped with a 25° field-of-view optical fiber pointing downward to measure the upwelling radiance of the crop. The position of the radiometer above the top of canopy was kept around 5.4 m throughout the growing season, yielding a circular sampling area with a diameter of around 2.4 m. The second radiometer was equipped with an optical fiber and a cosine diffuser (yielding a hemispherical field of view) pointing upward to simultaneously measure incident downwelling irradiance. Reflectance was then calculated as the ratio of measured upwelling radiance to downwelling irradiance (details in Gitelson et al., 2006b).

The radiometric data were collected close to solar noon (between 1100 and 1300 h local time) when changes in solar zenith angle were minimal. For each measurement site, six randomly selected plots were established, each with six randomly selected sampling points (details in Viña et al., 2011). Thus, 36 points were sampled per site at each data acquisition, and the average reflectance of 36 measurements was used as the site-level canopy reflectance. Reflectance measurements at the canopy level were performed from May to October during eight growing seasons—173 data acquisitions all together. This resulted in a total of 314 reflectance spectra for maize and 145 spectra for soybean. The canopy reflectance collected in situ was simulated in the spectral bands of TM/ETM+, MERIS, MSI, and OLCI in the range of 400 to 1000 nm by calculating the average reflectance over the bandwidth of the respective bands, since their spectral response functions are close to rectangular (Drusch et al., 2012; Clevers and Gitelson, 2013).

Surface Reflectance Derived from Satellite Measurements

Satellite measurements were processed as in previously published papers estimating GPP and green LAI (Gitelson et al., 2012; Nguy-Robertson and Gitelson, 2015). Sixty Landsat images used in this study were standard L1t files (georegistered, orthorectified) from the U.S. Geological Survey collected from the growing seasons (May–September) of 2001 through 2008. The geodetic accuracy of the L1t product is typically within 30 m (Lee et al., 2004). The image digital numbers were converted to top-of-atmosphere (TOA) reflectance, and then atmospherically corrected to surface reflectance using the Landsat Ecosystem Disturbance Adaptive Processing System (LEDAPS) at NASA GSFC (Masek et al., 2006). LEDAPS surface reflectance products have been compared to in situ data from the Aerosol Robotic Network (AERONET) and to daily 500 m resolution surface reflectance products from the MODIS sensor aboard the NASA Terra spacecraft (Masek et al., 2006; Feng et al., 2012). The uncertainties associated with the calculated reflectance values appear to be within the uncertainty of the MODIS surface reflectance product (0.5% absolute reflectance or 5% of the recorded reflectance value) for normal aerosol loadings (τ at 550 nm < 0.5). Imagery collected over each study site

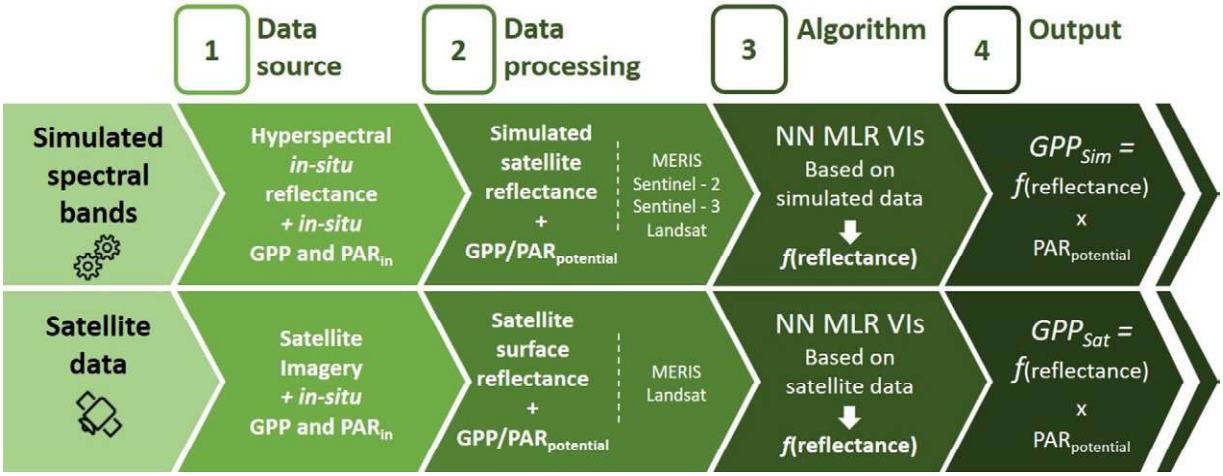

Fig. 1. Framework of estimating gross primary production (GPP) using in situ reflectance simulated in satellite spectral bands (Sim) and satellite surface reflectance data (Sat) together with potential photosynthetically active radiation ($PAR_{potential}$) by artificial neural network (NN), multiple linear regression (MLR), and vegetation indices (VI).

was subset using a rectangle polygon that encompasses approximately 500 pixels. These pixels were extracted from images, and the average value of all the per-pixel surface reflectance was used as the site-level reflectance.

The MERIS level 2 (MER_FR__2P) reflectance products (260 by 300 m) were collected between the growing seasons of 2003 through 2008 (49 images in total). Beam VISAT (v. 4.11, Brockmann Consult and contributors) was used to convert the Envisat N1 product to GeoTIFF and the remaining steps were completed in ArcGIS (v. 10.2, ESRI, Inc.) using Python's integrated development environment, IDLE, (v. 2.7.3 Python Software Foundation). Pixels where the quality control flags (band 32 in the MER_FR__2P product) indicated contamination (e.g., clouds, cloud shadows) or other issues (input/output errors) within 3 km (10 pixels) were removed. To reduce noise due to haze in imagery, pixels with aerosol optical thickness above 0.1 at 443 nm were excluded. The central pixel within the study site was used to avoid mixed pixels.

Data Analysis

Since total crop [Chl] can be retrieved from canopy reflectance (Gitelson et al., 2005), GPP was calculated based on Eq. [2] as:

$$GPP = f(\text{reflectance}) \times PAR_{potential} \quad [3]$$

where f(reflectance) is a function of reflectance collected in situ or derived from satellite observations used as a proxy of canopy [Chl]. The data set was composed from "clear sky" observations only. The value of $(PAR_{potential} - PAR_{in})/PAR_{potential}$ was used to indicate daily atmospheric conditions. In this study, clear sky conditions were defined when $(PAR_{potential} - PAR_{in})/PAR_{potential}$ <20%, resulting in 90% of the satellite images from the total data set available for use in this study (Gitelson et al., 2012).

The first stage of analysis was to improve the understanding of the GPP retrieval process by identifying uninformative spectral bands of the hyperspectral data. Uninformative variable elimination by partial least square regression (UVE-PLS) was used as an initial method to identify uninformative spectral bands in the hyperspectral data (Cai et al., 2008; Centner et al., 1996).

To indicate informative spectral bands, the reliability index (RI) was calculated as:

$$RI = \left| \frac{\overline{b_\rho}}{\text{std}(b_\rho)} \right| \quad [4]$$

where $\overline{b_\rho}$ is the value of the mean regression coefficient derived using four latent variables, and std (b_ρ) is the standard deviation of the regression coefficient vector. The number of latent variables was chosen to allow the model to extract general features of maize and soybean, assuming the potential spectral regions of interests are NIR, red edge and green, without overfitting the model with field specific features. The less informative the spectral band is the lower the RI value. The UVE-PLS was used separately on three data sets: maize, soybean, and maize and soybean combined to identify the informative bands for each crop species and to see if these informative bands are relevant in the combined set.

The data analysis framework (Fig. 1) was designed to explore the potential of estimating GPP using reflectance and $PAR_{potential}$. Two data sets were used- hyperspectral in situ reflectance simulating satellite reflectance bands (Sim) and satellite observations (Sat). The two data sets went through the same process of $GPP/PAR_{potential}$ estimation using a statistical model and reflectance bands, followed by a multiplication of $GPP/PAR_{potential}$ by $PAR_{potential}$ to retrieve GPP. Both Sim and Sat data sets underwent the same process of training and validation for estimating $GPP/PAR_{potential}$ using artificial NN (Wolpert, 1992), MLR (Bauer and Curran, 2005), and VIs. All three techniques were implemented using MATLAB (V. 9.4.0.813654, The MathWorks, Inc., Natick, MA).

The data processing was performed similarly to previously published papers estimating green LAI in these crops (Kira et al., 2016, 2017). Training and validation processes included the testing of all possible combinations of spectral bands and a 10-fold cross validation. To ensure a fair comparison between the results of the different techniques, the partition of subsets for cross validation was the same for all in situ data sets (Sim). Two main error measures were used to estimate the model performance during the 10-fold cross validation based on the comparison between estimated GPP and measured GPP: (i)

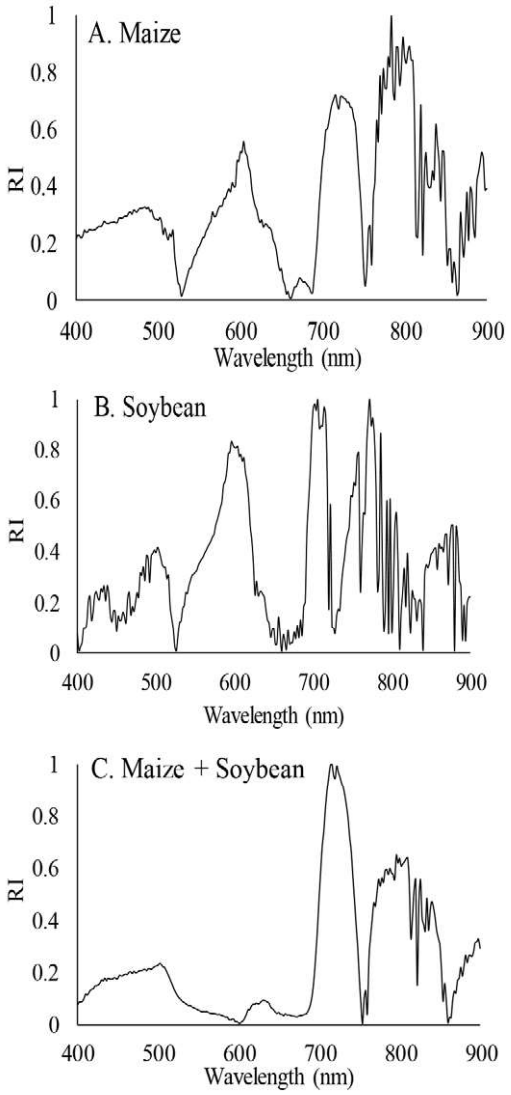

Fig. 2. Reliability index (RI), scaled between 0 and 1 (similar to input rescaling at neural network [NN] method), calculated by the uninformative variable elimination partial least squares (UVE-PLS) technique for gross primary production (GPP) estimation using hyperspectral in situ reflectance plotted vs. wavelength in (A) maize, (B) soybean, and (C) maize and soybean samples combined.

NRMSE which is the ratio of root mean square error and the average of measured GPP, (ii) coefficient of determination (R^2).

The same process was used for all methods of GPP estimation. First, a regression model was employed to estimate GPP/$PAR_{potential}$ using reflectance observations. Next, multiplying GPP/$PAR_{potential}$ by $PAR_{potential}$ the GPP value was retrieved. Two VI formulations were used (ρ_λ denotes reflectance at band λ, 400 nm < λ < 1000 nm): normalized difference (ND) = $(\rho_{\lambda 1}-\rho_{\lambda 2})/(\rho_{\lambda 1}+\rho_{\lambda 2})$, and chlorophyll index (CI) = $[(\rho_{\lambda 1}/\rho_{\lambda 2})-1]$ (Gitelson et al., 2003). λ_1 and λ_2 were tested with all possible bands and their combinations. The VIs were fitted to GPP/$PAR_{potential}$ using a parametric regression with both first and second order polynomials, and then multiplied by $PAR_{potential}$ to obtain GPP.

Unlike the use of VIs, MLR and NN were not limited to a specific number of bands. Both methods were used to develop the relationships between combinations of reflectance at different bands and GPP/$PAR_{potential}$. The non-parametric MLR fitted the reflectance bands to GPP/$PAR_{potential}$ using linear regression.

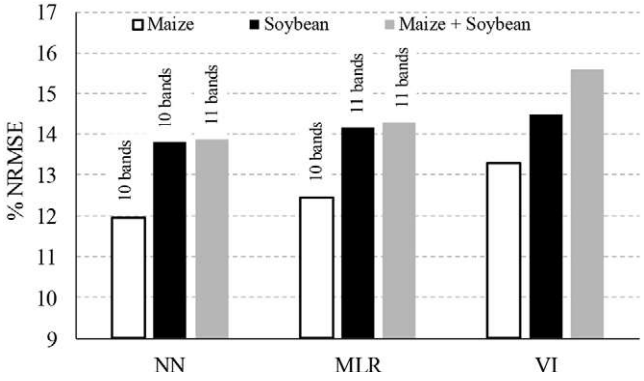

Fig. 3. Normalized root mean squared errors (NRMSE) of gross primary production (GPP) estimation by artificial neural network (NN), multiple linear regression (MLR), and vegetation index (VI) using in situ hyperspectral reflectance for maize, soybean, and for maize and soybean combined. Number of bands used by each method to achieve minimal NRMSE is presented on top of the bars. VIs used two bands

The NN fitted the reflectance bands to GPP/$PAR_{potential}$ using nonlinear relationships. The NN used in this study was a standard two-layer feed forward NN with a sigmoid transfer function. The data (input and output) were first rescaled in the range between 0 and 1 (the minimum value was subtracted from each input or output and the result was divided by the range between minimum and maximum values), and then trained and validated using training parameters and stopping criteria as performance error $<10^{-5}$ and minimal gradient $<10^{-15}$ (Kira et al., 2016, Kira et al., 2017). After a short optimization process, two hidden nodes were chosen to allow optimal estimation without overfitting the trained reflectance to the corresponding GPP/$PAR_{potential}$.

RESULTS

The UVE-PLS analysis was used to identify the informative spectral regions of hyperspectral in situ reflectance (400–1000 nm) for daily GPP estimation. For all three data sets (152 samples of maize, 79 samples of soybean, and maize and soybean combined), the reliability index was high at red edge (700–740 nm) and NIR (760–860 nm) spectral ranges indicating that the reflectance in these regions were informative for GPP estimation (Fig. 2). The RI was low in the blue (400–500 nm) and the red (650–690 nm), that is, the main spectral ranges of Chl absorption. For maize and soybean data sets, RI values in the green (520–630 nm) were high (Fig. 2A and 2B), but when samples of the two crops were taken together RI in the green considerably decreased (Fig. 2c). Thus, UVE-PLS indicated that the most informative spectral bands for GPP estimation in two crops combined were red edge and NIR.

Using in situ hyperspectral reflectance (251 bands), we tested reflectance at all possible band combinations for estimating GPP by NN, MLR, and VI and explored the band combinations with minimal NRMSE for each method. For the three tested data sets (maize, soybean, and maize and soybean combined), NN provided the most accurate estimation of GPP in both crops taken together with NRMSE below 14%. The NRMSE of MLR was below 15% and VI had higher NRMSE (Fig. 3). To gain the most accurate GPP estimations for maize and soybean separately, NN and MLR selected 10 to 11 bands with one band in the visible range, at least one red edge band, and several NIR bands.

Table 1. Algorithms, determination coefficient (R^2), and normalized root mean square errors (NRMSE in percent) of gross primary production (GPP) estimation by vegetation indices (VIs) in maize, soybean, and maize and soybean combined using in situ hyperspectral reflectance.

Data set	Algorithm	R^2	NRMSE
			%
Maize	$GPP = [3.83 \times (\rho_{762} - \rho_{724})/(\rho_{762} + \rho_{724}) - 0.01] \times PAR_{potential}$†	0.92	13.3
Soybean	$GPP = [1.79 \times (\rho_{732} - \rho_{704})/(\rho_{732} + \rho_{704}) + 0.07] \times PAR_{potential}$	0.91	14.5
Maize + soybean	$GPP = [4.82 \times (\rho_{766} - \rho_{730})/(\rho_{766} + \rho_{730}) - 0.02] \times PAR_{potential}$	0.91	15.6

† $PAR_{potential}$, potential photosynthetically active radiation.

For maize and soybean combined, at least one red edge band and several NIR bands were selected. The VI employing two bands was able to estimate GPP in two crops combined with NRMSE below 16% (Fig. 3). The best VIs for GPP estimation consistently used bands in NIR and red edge; soybean-specific models used both bands in the red edge region (Table 1).

Table 2 shows the results of GPP estimation by VI in maize and soybean combined using both in situ reflectance simulated in spectral bands of satellite sensors and surface reflectance products of satellites. For data contained in the OLCI, MSI, and MERIS spectral bands, the VI optimal spectral bands were consistently in NIR and red edge. Notably, VIs using long wavelength red edge reflectance around 730 to 740 nm yielded better accuracies than VIs using short red edge wavelength around 700 to 710 nm. For data contained in TM/ETM+ bands, the best VI used green and NIR reflectance.

For all tested band settings, NN was more accurate than VI (2–4% NRMSE decrease) for estimating GPP (Table 2, Fig. 4). The NRMSE of NN estimation using simulated MSI, OLCI, and MERIS data (with five to seven bands) was around 15%. To achieve minimal NRMSE for all data sets tested, NN consistently retained bands in the red edge and NIR regions (Tables 3 and 4). The accuracy of GPP estimation using in situ simulated reflectance was higher than that estimated using satellite surface reflectance products (Fig. 4).

With an increase in the number of bands retained by NN, NRMSE decreased. For all band settings, the general trend of NRMSE change was a sharp decrease as the number of retained bands reached three or four. Thereafter the rate of NRMSE decrease dropped and additional bands yielded only slight NRMSE decreases (Fig. 5).

For the cases where a single reflectance band was retained by NN using MSI, OLCI, or MERIS simulated data, the red edge carried the most predictive capability (e.g., Tables 3 and 4), explaining more than 78% of GPP variation. With two bands retained (one red edge band and one NIR band), R^2 increased up to 0.87. Three band algorithms retained red edge, NIR, and either an additional NIR or a green band. Such algorithms, with three retained bands, explained more than 90% of GPP variation (e.g., Tables 3 and 4). The accuracy of algorithms utilizing more than three bands increased slightly. The additional bands selected were usually located in the NIR region. NRMSE of the MSI five-band algorithm was 0.4% lower than that of the three-band (Table 3). The use of a longwave red edge band (such as MSI 740 nm) brought a higher accuracy than the use of a short wave red edge band (such as MSI 705 nm band, OLCI 709 nm band, and MERIS 705 nm band)–Tables 3 and 4. The model using MERIS satellite products retained six bands and was able to accurately estimate GPP with NRMSE = 18.7%, which indicates the good potential of using OLCI, onboard Sentinel 3, and MSI, onboard Sentinel 2, satellite products for GPP estimation in different crops. For both Landsat simulated data and Landsat reflectance products which lack red edge bands, NN selected blue, green, and NIR bands to achieve minimal NRMSE; however, this yielded much higher estimation errors (more than 24%) for GPP estimation in maize and soybean combined (Table 5).

DISCUSSION AND CONCLUSIONS

The green and NIR reflectance bring important information relating to GPP in maize and soybean-reliability index values were high in the green and NIR regions (Fig. 2a and 2b). Algorithms based on the reflectance in the green and NIR regions do allow accurate GPP assessment in soybean and maize separately (see also Gitelson et al., 2012). However, when maize and soybean data were taken together, the RI value in the green dropped (Fig. 2c) showing that such algorithms are species specific resulting in higher uncertainties (NRMSE around 25%) for the two crops combined (Fig. 4). Thus, accurate land cover maps that differentiate between crop types may be required to apply these algorithms at a regional scale.

The NN and VI algorithms using red edge and NIR bands were able to estimate GPP accurately in maize and soybean combined. Such algorithms not requiring re-parameterization for different vegetation species were found and explained in previous studies estimating Chl content (Gitelson et al., 2005), green LAI (Viña et al., 2011; Nguy-Robertson et al., 2014; Kira et al., 2017)

Table 2. Algorithms, determination coefficient (R^2), and normalized root mean squared errors (NRMSE in %) of gross primary production (GPP) estimation by vegetation index (VI) in maize and soybean combined using (a) simulated reflectance (Sim) in multispectral imager (MSI) (Sentinel-2), ocean and land color instrument (OLCI) (Sentinel-3), medium resolution imaging spectrometer (MERIS) (Envisat), thematic mapper or enhanced thematic mapper plus (TM/ETM+) (Landsat) bands, and (b) surface reflectance products of MERIS and Landsat satellites (Sat).

Sensor	Algorithm	R^2	NRMSE
			%
MSI (Sim)	$GPP = [8.77 \times (\rho_{783} - \rho_{740})/(\rho_{783} + \rho_{740}) - 0.02] \times PAR_{potential}$†	0.88	18.2
OLCI (Sim)	$GPP = [-0.022 \times (\rho_{779}/\rho_{709} - 1)^2 + 0.42 \times (\rho_{779}/\rho_{709} - 1) + 0.18] \times PAR_{potential}$	0.87	18.9
MERIS (Sim)	$GPP = [-0.016 \times (\rho_{775}/\rho_{705} - 1)^2 + 0.39 \times (\rho_{775}/\rho_{705} - 1) + 0.20] \times PAR_{potential}$	0.86	19.4
MERIS (Sat)	$GPP = [-0.077 \times (\rho_{754}/\rho_{705} - 1)^2 + 0.76 \times (\rho_{754}/\rho_{705} - 1) - 0.052] \times PAR_{potential}$	0.85	20.4
TM/ETM+ (Sim)	$GPP = [-0.014 \times (\rho_{830}/\rho_{560} - 1)^2 + 0.32 \times (\rho_{830}/\rho_{560} - 1) - 0.12] \times PAR_{potential}$	0.80	24.9
TM/ETM+ (Sat)	$GPP = [-0.020 \times (\rho_{830}/\rho_{560} - 1)^2 + 0.40 \times (\rho_{830}/\rho_{560} - 1) - 0.36] \times PAR_{potential}$	0.80	25.7

† $PAR_{potential}$, potential photosynthetically active radiation.

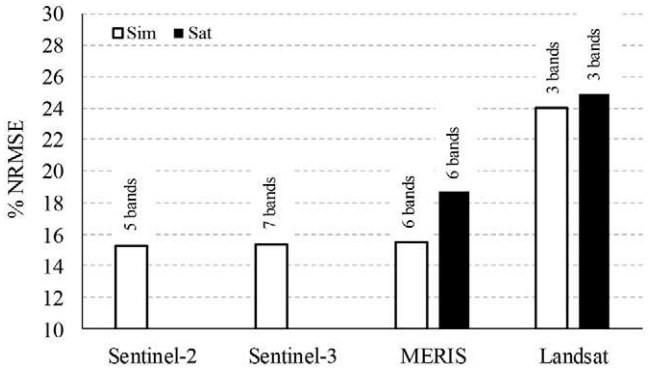

Fig. 4. Normalized root mean square errors (NRMSE) of gross primary production (GPP) estimation in maize and soybean combined by using artificial neural network (NN) with simulated reflectance (Sim) of multispectral imager (MSI) (Sentinel-2), ocean and land color instrument (OLCI) (Sentinel-3), TM/ETM+ (Landsat), and satellite derived reflectance (Sat) from thematic mapper or enhanced thematic mapper plus (TM/ETM+) (Landsat) and medium resolution imaging spectrometer (MERIS) data. Number of bands retained by NN is shown on top of the bars.

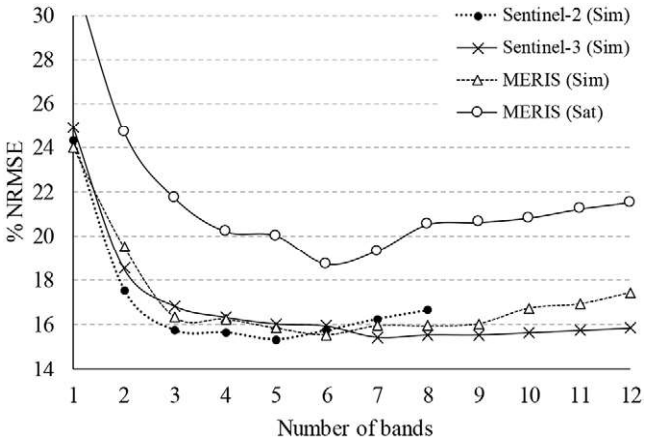

Fig. 5. Normalized root mean square errors (NRMSE) of gross primary production (GPP) estimation by artificial neural network (NN) in maize and soybean combined plotted vs. the band number using simulated multispectral imager (MSI) (Sentinel-2), ocean and land color instrument (OLCI) (Sentinel-3), as well as the surface reflectance medium resolution imaging spectrometer (MERIS) product.

and GPP (Gitelson, 2011, 2018; Peng and Gitelson, 2012). The NN and VIs, using red edge bands around 720 to 740 nm, available in MSI (Sentinel-2), allowed for 1 to 2% increase in accuracy compared to red edge bands around 705 to 709 nm, available in MSI (Sentinel-2), OLCI (Sentinel-3), and previously available in MERIS. This agrees with the findings that red edge NDVI and red edge chlorophyll index employing reflectance around 720 to 730 nm are able to most accurately estimate total canopy [Chl] (Gitelson et al., 2005) and GPP (Peng and Gitelson, 2012).

Compared to VI, NN makes use of more bands to improve model accuracy. When more than three or four bands in simulated data were retained in the NN model, the accuracy of GPP estimation increased only slightly. Besides one red edge and one NIR band, in most cases NN tended to select several additional NIR bands. This is consistent with observations of many studies; namely, in addition to a red edge band the most often selected bands for LAI estimation by NN were located in the NIR region (Richter et al., 2012; Verger et al., 2011; Verrelst et al., 2013, 2016; Berger et al., 2018). The inclusion of additional NIR bands may better indicate multiple and complex canopy scattering related to crop structure (monoculture and row structure). For all tested spectral band settings, however, using too many bands in NN decreased model accuracy (Fig. 5), since some bands may contain additional noise and the spectral redundancy may outweigh the information gain. The use of too many bands may also cause over-fitting of the model to the trained data. Several studies have demonstrated that estimation accuracy was higher when using several defined spectral bands than when using the full spectral information available from a sensor (Meroni et al., 2004; Darvishzadeh et al., 2008; Verrelst et al., 2013, 2016; Kira et al., 2017).

The crop samples tested in this study represented contrasting species (maize and soybean), different environmental conditions (irrigated and rainfed during 8 yr of observation) and varying phenological stages (vegetative and reproductive). The results showed that three–five band combination (NN) and the two-band (VIs) including red edge and NIR are optimal for GPP estimation with minimum band number by all methods tested here for both rainfed and irrigated maize and soybean during the entire growing season. These selected bands coincide with the bands found to be optimal for estimating canopy [Chl] as noted in many studies (e.g., Gitelson et al., 2003; Dash and Curran, 2004; Gitelson et al., 2005). This confirms that canopy [Chl] is the factor governing GPP in croplands as LUE has been found to be conservative in rainfed and irrigated crops (Gitelson et al., 2016, 2018). This result allows a simple model to be used for estimating GPP via canopy [Chl] based on solely remotely sensed data.

The conclusions are summarized as follows:

Table 3. Determination coefficients (R^2), normalized root mean squared errors (NRMSE) of gross primary production (GPP) estimation by artificial neural network (NN) in maize and soybean combined with different band numbers. The analysis was conducted on reflectance simulated in multispectral imager (MSI) bands.

Band no.	R^2	NRMSE	Simulated MSI bands							
		%	Central wavelength, nm							
1	0.79	24.3	740							
2	0.89	17.5	740	783						
3	0.91	15.7	740	783	842					
4	0.91	15.6	665	740	783	842				
5	0.92	15.3	665	705	740	783	842			
6	0.91	15.7	490	665	705	740	783	842		
7	0.91	16.2	560	665	705	740	783	842	865	
8	0.90	16.6	490	560	665	705	740	783	842	865

Table 4. Determination coefficients (R^2), normalized root mean squared errors (NRMSE) of gross primary production (GPP) estimation by artificial neural network (NN) in maize and soybean combined with different band numbers. The analysis was conducted on reflectance simulated in ocean and land color instrument (OLCI) bands.

Band no.	R^2	NRMSE	Simulated OLCI bands																			
		%	Central wavelength, nm																			
1	0.78	24.9	709																			
2	0.88	18.5	709	764																		
3	0.90	16.8	560	709	764																	
4	0.91	16.3	665	709	779	940																
5	0.91	16.0	560	682	709	865	940															
6	0.91	15.9	490	620	709	754	767	900														
7	0.92	15.4	443	754	764	767	779	865	940													
8	0.92	15.5	490	560	754	767	779	865	885	940												
9	0.92	15.5	620	709	754	764	767	779	865	885	900											
10	0.92	15.6	620	709	754	764	767	779	865	885	900	940										
11	0.91	15.7	400	674	682	709	754	764	767	779	865	885	940									
12	0.91	15.8	674	682	709	754	764	767	779	865	865	885	900	940								
13	0.91	15.9	413	620	665	674	682	709	754	764	779	865	885	900	940							
14	0.91	15.9	400	490	620	674	682	709	754	761	764	767	779	885	900	940						
15	0.91	16.2	400	510	560	620	665	674	682	709	754	761	767	779	865	900	940					
16	0.91	16.2	400	400	560	620	665	674	682	709	754	761	764	767	779	865	885	900				
17	0.91	16.2	490	510	560	620	665	674	682	709	754	754	764	767	779	865	885	900	940			
18	0.90	16.6	443	490	510	620	620	665	674	682	709	754	761	764	767	779	865	885	900	940		
19	0.90	16.6	400	413	490	560	620	665	674	682	709	754	761	764	767	779	865	885	885	900	940	
20	0.90	17.0	400	413	490	510	510	560	620	665	674	682	709	754	761	764	767	779	865	885	900	940

1. Neural network was able to accurately estimate GPP in maize and soybean combined with no re-parameterization with NRMSE below 16% using simulated MSI, OLCI, MERIS data, and below 19% using the MERIS satellite product.
2. For the three techniques tested, NN, MSR, and VI, using a few optimal spectral bands yielded more accurate GPP estimations than when using all possible bands of hyper-spectral data.
3. For all tested spectral settings, the bands selected by NN, MSR, and VI for GPP estimation in the two crops combined consistently included bands in the NIR and red edge regions.
4. Vegetation indices based on red edge and NIR reflectance were simple and efficient for non-species specific GPP estimation in both crops combined.

ACKNOWLEDGMENTS

The US-Ne1, US-Ne2, and US-Ne3 AmeriFlux sites are supported by the Lawrence Berkeley National Lab AmeriFlux Data Management Program and by the Carbon Sequestration Program, University of Nebraska-Lincoln Agricultural Research Division. Funding for AmeriFlux core site data was provided by the U.S. Department of Energy's Office of Science. Partial support from the Nebraska Agricultural Experiment Station with funding from the Hatch Act (accession no. 1002649) through the USDA National Institute of Food and Agriculture is also acknowledged. Y. Peng was supported by National Natural Science Foundation of China (no. 41771381). O. Kira was supported by BARD, the United States-Israel Binational Agricultural Research and Development Fund, Vaadia-BARD Postdoctoral Fellowship Award no. FI-576-18.

Table 5. Determination coefficients (R^2), normalized root mean square error (NRMSE) of gross primary production (GPP) estimation by neural network (NN) in maize and soybean combined with different band numbers. The analysis was conducted on surface reflectance products derived from Landsat satellite images.

Band no.	R^2	NRMSE	Satellite TM/ETM+ bands†			
		%	Central wavelength, nm			
1	0.78	26.7	660			
2	0.79	26.1	660	830		
3	0.80	24.9	485	560	660	
4	0.79	25.5	485	560	660	830

† TM/ETM+, thematic mapper or enhanced thematic mapper plus.

REFERENCES

Allen, W.A., H.W. Gausman, and A.J. Richardson. 1973. Willstatter-Stoll theory of leaf reflectance evaluated by ray tracing. Appl. Opt. 12(10):2448–2453. doi:10.1364/AO.12.002448

Baldocchi, D.D. 2003. Assessing the eddy covariance technique for evaluating carbon dioxide exchange rates of ecosystems: Past, present and future. Glob. Change Biol. 9:479–492. doi:10.1046/j.1365-2486.2003.00629.x

Bauer, D.J., and P.J. Curran. 2005. Probing interactions in fixed and multilevel regression: Inferential and graphical techniques. Multivariate Behav. Res. 40:373–400. doi:10.1207/s15327906mbr4003_5

Berger, K., C. Atzberger, M. Danner, M. Wocher, W. Mauser, and T. Hank. 2018. Model-based optimization of spectral sampling for the retrieval of crop variables with the PROSAIL model. Remote Sens. 10(12). doi:10.3390/rs10122063

Cai, W., Y. Li, and X. Shao. 2008. A variable selection method based on uninformative variable elimination for multivariate calibration of near-infrared spectra. Chemom. Intell. Lab. Syst. 90:188–194. doi:10.1016/j.chemolab.2007.10.001

Centner, V., D.L. Massart, O.E. de Noord, S. de Jong, B.M. Vandeginste, and C. Sterna. 1996. Elimination of uninformative variables for multivariate calibration. Anal. Chem. 68:3851–3858. doi:10.1021/ac960321m

Ciganda, V., A.A. Gitelson, and J. Schepers. 2009. Non-destructive determination of maize leaf and canopy chlorophyll content. J. Plant Physiol. 166:157–167. doi:10.1016/j.jplph.2008.03.004

Clevers, J.G.P.W., and A.A. Gitelson. 2013. Remote estimation of crop and grass chlorophyll and nitrogen content using red-edge bands on Sentinel-2 and -3. Int. J. Appl. Earth Obs. Geoinf. 23:344–351. doi:10.1016/j.jag.2012.10.008

Darvishzadeh, R., A. Skidmore, M. Schlerf, and C. Atzberger. 2008. Inversion of a radiative transfer model for estimating vegetation LAI and chlorophyll in a heterogeneous grassland. Remote Sens. Environ. 112(5):2592–2604. doi:10.1016/j.rse.2007.12.003

Dash, J., and P.J. Curran. 2004. The MERIS terrestrial chlorophyll index. Int. J. Remote Sens. 25:5403–5413. doi:10.1080/0143116042000274015

Dorigo, W.A., R. Zurita-Milla, A.J.W. de Wit, J. Brazile, R. Singh, and M.E. Schaepman. 2007. A review on reflective remote sensing and data assimilation techniques for enhanced agroecosystem modeling. Int. J. Appl. Earth Obs. Geoinf. 9:165–193. doi:10.1016/j.jag.2006.05.003

Drusch, M., U.D. Bello, S. Carlier, O. Colin, V. Fernandez, F. Gascon et al. 2012. Sentinel-2: Esa's optical high-resolution mission for gmes operational services. Remote Sens. Environ. 120(1):25–36. doi:10.1016/j.rse.2011.11.026

D'Urso, G., K. Richter, A. Calera, M.A. Osann, R. Escadafal, J. Garatuza-Pajan et al. 2010. Earth observation products for operational irrigation management in the context of the pleiades project. Agric. Water Manage. 98:271–282. doi:10.1016/j.agwat.2010.08.020

Feng, M., C. Huang, S. Channan, E. Vermote, J. Masek, and J.R. Townshend. 2012. Quality assessment of Landsat surface reflectance products using MODIS data. Comput. Geosci. 38:9–22. doi:10.1016/j.cageo.2011.04.011

Gitelson, A.A. 2004. Wide dynamic range vegetation index for remote quantification of crop biophysical characteristics. J. Plant Physiol. 161:165–173. doi:10.1078/0176-1617-01176

Gitelson, A.A. 2011. Remote sensing estimation of crop biophysical characteristics at various scales. In: P.S. Thenkabail, J.G. Lyon, and A. Huete, editors, Hyperspectral remote sensing of vegetation. CRC Press, Taylor and Francis, Boca Raton, FL. p. 329–358. doi:10.1201/b11222-21

Gitelson, A.A. 2018. Recent developments in remote estimation of crop biophysical and biochemical properties at various scales. In: P.S. Thenkabail, J.G. Lyon, and A. Huete, editors, Hyperspectral remote sensing of vegetation. Vol. III. CRC Press, Taylor and Francis, Boca Raton, FL. p. 3–24.

Gitelson, A.A., T. Arkebauer, and A.E. Suyker. 2018. Convergence of daily light use efficiency in irrigated and rainfed C3 and C4 crops. Remote Sens. Environ. 217:30–37. doi:10.1016/j.rse.2018.08.007

Gitelson, A.A., U. Gritz, and M.N. Merzlyak. 2003. Relationships between leaf chlorophyll content and spectral reflectance and algorithms for non-destructive chlorophyll assessment in higher plant leaves. J. Plant Physiol. 160(3):271–282. doi:10.1078/0176-1617-00887

Gitelson, A.A., G.P. Keydan, and M.N. Merzlyak. 2006b. Three-band model for noninvasive estimation of chlorophyll, carotenoids, and anthocyanin contents in higher plant leaves. Geophys. Res. Lett. 33:L11402. doi:10.1029/2006GL026457

Gitelson, A.A., Y. Peng, J.G. Masek, D.C. Rundquist, S.B. Verma, A. Suyker et al. 2012. Remote estimation of crop gross primary production with Landsat data. Remote Sens. Environ. 121:404–414. doi:10.1016/j.rse.2012.02.017

Gitelson, A.A., Y. Peng, D.C. Rundquist, A. Suyker, and S.B. Verma. 2015. Remote estimation of gross primary productivity in maize and soybean: From close range to satellites. In: J.V. Stafford, editor, Precision agriculture'15. Wageningen Academic Publishers, the Netherlands. p. 183–190. doi:10.3920/978-90-8686-814-8_22

Gitelson, A.A., Y. Peng, A. Viña, T. Arkebauer, and J.S. Schepers. 2016. Efficiency of chlorophyll in gross primary productivity: A proof of concept and application in crops. J. Plant Physiol. 201:101–110. doi:10.1016/j.jplph.2016.05.019

Gitelson, A.A., A. Viña, V. Ciganda, D.C. Rundquist, and T.J. Arkebauer. 2005. Remote estimation of canopy chlorophyll content in crops. Geophys. Res. Lett. 32:L08403. doi:10.1029/2005GL022688

Gitelson, A.A., A. Viña, S.B. Verma, D.C. Rundquist, T.J. Arkebauer, G. Keydan et al. 2006a. Relationship between gross primary production and chlorophyll content in crops: Implications for the synoptic monitoring of vegetation productivity. Geophys. Res. Lett. 111:D08S11. doi:10.1029/2005JD006017

Hank, T.B., K. Berger, H. Bach, J.G.P.W. Clevers, A. Gitelson, P. Zarco-Tejada, and W. Mauser. 2019. Spaceborne imaging spectroscopy for sustainable agriculture: Contributions and challenges. Surv. Geophys. 40 (3):515–551.

Harris, A., and J. Dash. 2010. The potential of the MERIS Terrestrial chlorophyll Index for carbon flux estimation. Remote Sens. Environ. 114:1856–1862. doi:10.1016/j.rse.2010.03.010

Kira, O., A.L. Nguy-Robertson, T.J. Arkebauer, R. Linker, and A.A. Gitelson. 2016. Informative spectral bands for remote green LAI estimation in C3 and C4 crops. Agric. For. Meteorol. 218-219:243–249. doi:10.1016/j.agrformet.2015.12.064

Kira, O., A.L. Nguy-Robertson, T.J. Arkebauer, R. Linker, and A.A. Gitelson. 2017. Toward generic models for green LAI estimation in maize and soybean: Satellite observations. Remote Sens. 9:318. doi:10.3390/rs9040318

Lee, D.S., J.C. Storey, M.J. Choate, and R. Hayes. 2004. Four years of Landsat-7 on-orbit geometric calibration and performance. IEEE Trans. Geosci. Remote Sens. 42:2786–2795. doi:10.1109/TGRS.2004.836769

Masek, J.G., E.F. Vermote, N. Saleous, R. Wolfe, F.G. Hall, F. Huemmrich et al. 2006. A Landsat surface reflectance data set for North America. 1990-2000. IEEE Geosci. Remote Sens. Lett. 3:68–72. doi:10.1109/LGRS.2005.857030

Medina, E., and H. Lieth. 1964. Die Beziehungen zwischen Chlorophyllgehalt, assimilierender Flaeche und Trockensubstanzproduktion in einigen Pflanzengemeinschaften. (The relationships between chlorophyll content, assimilating area and dry matter production in some plant communities.). Beitr. Biol. Pflanzen. 40:451–494.

Meroni, M., R. Colombo, and C. Panigada. 2004. Inversion of a radiative transfer model with hyperspectral observations for LAI mapping in poplar plantations. Remote Sens. Environ. 92(2):195–206. doi:10.1016/j.rse.2004.06.005

Nguy-Robertson, A.L., and A.A. Gitelson. 2015. Algorithms for estimating green leaf area index in C3 and C4 crops for MODIS, Landsat TM/ETM+, MERIS, Sentinel MSI/OLCI, and Venμs sensors. Remote Sens. Lett. 6(5):360–369. doi:10.1080/2150704X.2015.1034888

Nguy-Robertson, A.L., Y. Peng, A.A. Gitelson, T.J. Arkebauer, A. Pimstein, I. Herrmann et al. 2014. Estimating green LAI in four crops: Potential of determining optimal spectral bands for a universal algorithm. Agric. For. Meteorol. 192-193:140–148. doi:10.1016/j.agrformet.2014.03.004

Nguy-Robertson, A., A.E. Suyker, and X. Xiao. 2015. Modeling gross primary production of maize and soybean croplands using light quality, temperature, water stress, and phenology. Agric. For. Meteorol. 213:160–172. doi:10.1016/j.agrformet.2015.04.008

Peng, Y., and A.A. Gitelson. 2012. Remote estimation of gross primary productivity in soybean and maize based on total crop chlorophyll content. Remote Sens. Environ. 117:440–448. doi:10.1016/j.rse.2011.10.021

Peng, Y., A.A. Gitelson, G. Keydan, D.C. Rundquist, and W. Moses. 2011. Remote estimation of gross primary production in maize and support for a new paradigm based on total crop chlorophyll content. Remote Sens. Environ. 115:978–989. doi:10.1016/j.rse.2010.12.001

Peng, Y., A.A. Gitelson, and T. Sakamoto. 2013. Remote estimation of gross primary productivity in crops using MODIS 250 m data. Remote Sens. Environ. 128(21):186–196. doi:10.1016/j.rse.2012.10.005

Reeves, M.C., M. Zhao, and S.W. Running. 2005. Usefulness and limits of MODIS GPP for estimating wheat yield. Int. J. Remote Sens. 26(7):1403–1421. doi:10.1080/01431160512331326567

Richter, K., T.B. Hank, F. Vuolo, W. Mauser, and G. D'Urso. 2012. Optimal exploitation of the sentinel-2 spectral capabilities for crop leaf area index mapping. Remote Sens. 4(3):561–582. doi:10.3390/rs4030561

Rossini, M., M. Migliavacca, M. Galvagno, M. Meroni, S. Cogliati, E. Cremonese et al. 2014. Remote estimation of grassland gross primary production during extreme meteorological seasons. Int. J. Appl. Earth Obs. Geoinf. 29:1–10. doi:10.1016/j.jag.2013.12.008

Rundquist, D.C., A.A. Gitelson, B. Leavitt, A. Zygielbaum, R. Perk, and G.P. Keydan. 2014. Elements of an integrated phenotyping system for monitoring crop status at canopy level. Agronomy (Basel) 4(1):108–123. doi:10.3390/agronomy4010108

Rundquist, D.C., R. Perk, B. Leavitt, G.P. Keydan, and A.A. Gitelson. 2004. Collecting spectral data over cropland vegetation using machine-positioning versus hand-positioning of the sensor. Comput. Electron. Agric. 43:173–178. doi:10.1016/j.compag.2003.11.002

Sakamoto, T., A.A. Gitelson, B.D. Wardlow, S.B. Verma, and A.E. Suyker. 2011. Estimating daily gross primary production of maize based only on MODIS WDRVI and shortwave radiation data. Remote Sens. Environ. 115:3091–3101. doi:10.1016/j.rse.2011.06.015

Sakowska, K., L. Vescovo, B. Marcolla, R. Juszczak, J. Olejnik, and D. Gianelle. 2014. Monitoring of carbon dioxide fluxes in a subalpine grassland ecosystem of the Italian alps using a multispectral sensor. Biogeosciences 11(17):4695–4712. doi:10.5194/bg-11-4695-2014

Suyker, A.E., S.B. Verma, G.G. Burba, and T.J. Arkebauer. 2005. Gross primary production and ecosystem respiration of irrigated maize and irrigated soybean during a growing season. Agric. For. Meteorol. 131:180–190. doi:10.1016/j.agrformet.2005.05.007

Thenkabail, P.S., J.G. Lyon, and A. Huete. 2011. Hyperspectral remote sensing of vegetation. CRC Press, Taylor and Francis, Boca Raton, FL.

Turner, D.P., S. Urbanski, D. Bremer, S. Wofsy, T. Meyers, S.T. Gower et al. 2003. A cross-biome comparison of daily light use efficiency for gross primary production. Glob. Change Biol. 9:383–395. doi:10.1046/j.1365-2486.2003.00573.x

Ustin, S.L., M.O. Smith, S. Jacquemoud, M.M. Verstraete, and Y. Govaerts. 1999. GeoBotany: Vegetation mapping for earth sciences. In: A.N. Rencz, editor, Manual of remote sensing: Remote sensing for the earth sciences. 3rd ed. Vol. 3. p. 189–248.

Verger, A., F. Baret, and F. Camacho. 2011. Optimal modalities for radiative transfer-neural network estimation of canopy biophysical characteristics: Evaluation over an agricultural area with chris/proba observations. Remote Sens. Environ. 115:415–426. doi:10.1016/j.rse.2010.09.012

Verma, S.B., A. Dobermann, K.G. Cassman, D.T. Walters, J.M. Knops, T.J. Arkebauer et al. 2005. Annual carbon dioxide exchange in irrigated and rainfed maize-based agroecosystems. Agric. For. Meteorol. 131:77–96. doi:10.1016/j.agrformet.2005.05.003

Verrelst, J., L. Alonso, J. Rivera Caicedo, J. Moreno, and G. Camps-Valls. 2013. Gaussian process retrieval of chlorophyll content from imaging spectroscopy data. IEEE J. Sel. Top. Appl. Earth Obs. Remote Sens. 6(2):867–874. doi:10.1109/JSTARS.2012.2222356

Verrelst, J., J.P. Rivera, A. Gitelson, J. Delegido, J. Moreno, and G. Camps-Valls. 2016. Spectral band selection for vegetation properties retrieval using Gaussian processes regression. Int. J. Appl. Earth Obs. Geoinf. 52:554–567. doi:10.1016/j.jag.2016.07.016

Viña, A., A.A. Gitelson, A.L. Nguy-Robertson, and Y. Peng. 2011. Comparison of different vegetation indices for the remote assessment of green leaf area index of crops. Remote Sens. Environ. 115:3468–3478. doi:10.1016/j.rse.2011.08.010

Weiss, A., and J.M. Norman. 1985. Partitioning solar radiation into direct and diffuse, visible and near-infrared components. Agric. For. Meteorol. 34, 205–213.

Whittaker, R.H., and P.L. Marks. 1975. Methods of assessing terrestrial productivity. In: H. Lieth and R.H. Whittaker, editors, Primary productivity of the biosphere. Ecological studies. Vol. 14. Springer-Verlag, New York. p. 55–118.

Wolpert, D.H. 1992. Stacked generalization. Neural Netw. 5(2):241–259. doi:10.1016/S0893-6080(05)80023-1

Woolley, J.T. 1971. Reflectance and transmittance of light by leaves. Plant Physiol. 47:656–662. doi:10.1104/pp.47.5.656

Xu, L., and D.D. Baldocchi. 2003. Seasonal trends in photosynthetic parameters and stomatal conductance of blue oak (quercus douglasii) under prolonged summer drought and high temperature. Tree Physiol. 23(13):865–877. doi:10.1093/treephys/23.13.865

Zarco-Tejada, P.J., J.R. Miller, G.H. Mohammed, T.L. Noland, and P.H. Sampson. 2002. Vegetation stress detection through chlorophyll a + b estimation and fluorescence effects on hyperspectral imagery. J. Environ. Qual. 31:1433–1441.